# Optimization of Rapid Acquisition With Relaxation Enhancement (RARE) Pulse Sequence Parameters for $^{19}$F-MRI Studies

Alfonso Mastropietro, PhD,[1,2] Elisabetta De Bernardi, PhD,[1,3,4] Gian Luca Breschi, PhD,[5,8] Ileana Zucca, PhD,[2] Massimo Cametti, PhD,[7] Chiara Dolores Soffientini, MSc,[1] Marco de Curtis, MD,[5] Giancarlo Terraneo, PhD,[7] Pierangelo Metrangolo, PhD,[7] Roberto Spreafico, MD, PhD,[8] Giuseppe Resnati, PhD,[7] and Giuseppe Baselli, MSc[1]*

THE ADVENT of high field magnetic resonance scanners has made magnetic resonance imaging (MRI) a powerful investigation tool for molecular imaging (MI) (1). $^{1}$H-MRI can provide a wealth of functional, microstructural, and chemical information. This aspect is particularly important in neurological studies, where a correlation of metabolic or cell-tracking information with anatomical and functional information is needed (2,3). Hetero-nuclear MR studies (with $^{13}$C, $^{23}$Na, $^{31}$P, $^{19}$F nuclei) provide a direct means to trace molecular compounds in living tissues (4). In particular, $^{19}$F displays favorable properties such as 100% natural abundance, isotopic stability, high sensitivity (83% of $^{1}$H), limited shift of gyromagnetic ratio compared to $^{1}$H (40.05 MHz/T vs. 42.58 MHz/T), and virtually null background (5–9). Several works have recently addressed fluorinated reporters for integrated $^{1}$H/$^{19}$F MR molecular imaging studies (10–15).

However, the inherently low sensitivity of the MR technique is particularly critical in $^{19}$F-MRI experiments, considering the low amount of $^{19}$F atoms that can be foreseen in target tissues/structures (8,9). Therefore, to fully exploit the potential of $^{19}$F-MR in molecular imaging, it is necessary to: 1) adopt selective highly fluorinated reporters; 2) use high-

[1]Politecnico di Milano, Department of Electronics Information and Bioengineering, Milano, Italy.

[2]Scientific Direction Unit, Fondazione IRCCS Istituto Neurologico C. Besta, Milano, Italy.

[3]Health Science Department, University of Milano-Bicocca, Monza, Italy.

[4]Tecnomed Foundation, University of Milano-Bicocca, Monza, Italy.

[5]Experimental Neurophysiology and Epileptology Unit, Fondazione IRCCS Istituto Neurologico C. Besta, Milano, Italy.

[6]Politecnico di Milano, NFMLab Department of Chemistry, Materials and Chemical Engineering Giulio Natta, Milano, Italy.

[7]Clinical Epileptology and Experimental Neurophysiology Unit, Fondazione IRCCS Istituto Neurologico C. Besta, Milano, Italy.

[8]Department of Neuroscience and Brain Technologies, Istituto Italiano di Tecnologia, Genova, Italy.

Contract grant sponsor: Cariplo Foundation, project title: "New-Generation Fluorinated Materials as Smart Reporter Agents in $^{19}$F MRI" project no. 2009–2550; Contract grant sponsor: MIUR, FIRB project "Materiali Fluorurati Nanostrutturati come Mezzi di Contrasto Intelligenti in $^{19}$F RMN (FLUORIMAGING)" project no. RBAP1183B5.

*Address reprint requests to: G.B., Politecnico di Milano, Department of Bioengineering, Via Golgi 39, 20133 Milano, Italy.
E-mail: giuseppe.baselli@polimi.it

Received June 26, 2012; Accepted July 16, 2013.

performance hardware (eg, high magnetic fields, elevated coil sensitivities, etc.); and 3) optimize data collection sequences in order to improve the signal to noise ratio (SNR) and detection limits (16–18). This work deals with the last issue by proposing a data acquisition strategy set on the specific relaxation times of the investigated $^{19}F$ compound.

Given the generally long $T_1$ relaxation time of low-molecular-weight fluorinated compounds (19,20), fast imaging sequences (21) are useful for $^{19}F$-MRI, in order to increase the number of averages and hence the SNR. An efficient *k*-space sampling strategy (22) can add further improvement. Results described in literature deal with gradient echo sequences, such as fast low angle shot (FLASH), and spin echo sequences, such as rapid acquisition with relaxation enhancement (RARE, or fast spin echo) (23–27), with a considerable predominance of the latter. However, the performance of these sequences is largely dependent on the relaxation times of the addressed spin system, with large variations among different reporters (28,29).

Recently, different works have shown how an accurate pulse sequence optimization can improve the detection sensitivity in $^{19}F$ MRI studies (18,30,31). The main goal of this study is to provide a method to optimize the RARE sequence, given a specific set of relaxation times ($T_1$, $T_2$). The RARE sequence permits reducing the acquisition time by accumulating multiple echoes within a single repetition time (TR) (32). The use of driven equilibrium pulses, in combination with RARE, improves the SNR by reducing TR accordingly to the $T_1/T_2$ ratio (33,34). A specific study on $^{19}F$ MRI is mainly justified for two reasons: 1) in contrast with $^{1}H$ MRI, the focus of the $^{19}F$ MRI optimization process is the SNR and not the contrast-to-noise ratio (CNR), because of the lack of background signal from the biological tissue; and 2) owing to the large range of relaxation times, $^{19}F$ MRI requires a more reliable optimization process based on the $^{19}F$ compounds magnetic properties ($T_1$, $T_2$, $T_2$*).

In this work, an optimization method for RARE sequences using a 7T MRI scanner is proposed based on numerical simulations which take into account the previous evaluation of fluorinated compound relaxation times. The method was tested on potassium hexafluorophosphate ($KPF_6$) in different conditions: 1) water solution, 2) agarose mixture, and 3) previously perfused ex vivo guinea pig brain. Optimization maps for TR and ETL (echo train length) are provided in different $T_1$ and $T_2$ conditions at fixed TE.

## MATERIALS AND METHODS

### *RARE Pulse Sequence: Theoretical Assessment of SNR and Optimal Parameters*

The SNR in an MR image is defined as the ratio between the amplitude of the signal and the standard deviation of the noise (35).

The SNR can be expressed as:

$$SNR \propto \Delta x \Delta y \Delta z \cdot \frac{S_{avg}}{N_{freq}} \cdot \sqrt{\frac{NA * N_{freq} \cdot N_{phase}}{BW}} \qquad [1]$$

where $S_{avg}$ is the average of the signal and depends on the specific pulse sequence and $N_{freq}$ is the number of frequency-encoded samples, $N_{phase}$ is the number of phase-encoded samples, NA is the number of averages, and $BW = 1/(N_{freq}*T_s)$ is the receiver bandwidth; ($T_s$ is the sampling time).

In a RARE pulse sequence, for a steady state condition, $S_{avg}$ can be approximated by considering the amplitude of the registered echoes in a single repetition of the sequence as:

$$S_{avg} = \frac{1}{ETL} \sum_{n=1}^{ETL} M_{xy}^{Steady\_State} \cdot \exp\left(\frac{-n \cdot \Delta TE}{T_2}\right) \qquad [2]$$

where $M_{xy}^{Steady\_State}$ is the value of the steady-state transverse magnetization at the beginning of the pulse sequence repetition and ΔTE is the echo spacing. The amplitude of the registered echoes is influenced by the magnetic properties of the acquired samples (ie, longitudinal and transversal relaxation time constants $T_1$ and $T_2$) and by the parameters of the RARE pulse sequence, which are:

- repetition time (TR);
- number of echoes collected during each repetition (echo train length [ETL] or RARE-factor);
- activation or deactivation of driven equilibrium pulses, ie, flip back of the residual magnetization in TR (conditions indicated in the following as FB ON and FB OFF, respectively).

If we consider a fixed total acquisition time TA, the number of averages NA can be expressed as:

$$NA = \frac{TA}{TR} \cdot \frac{ETL}{N_{phase}} \qquad [3]$$

Therefore, by substituting in Eq. [4] we have:

$$SNR \propto \Delta x \cdot \Delta y \cdot \Delta z \cdot \sum_{n=1}^{ETL} M_{xy}^{Steady\_State} \cdot \exp\left(\frac{-n \cdot \Delta TE}{T_2}\right) \cdot \frac{\sqrt{TA \cdot N_{freq}}}{\sqrt{TR \cdot ETL \cdot BW}} \qquad [4]$$

Starting from a longitudinal equilibrium magnetization $M^0_z$, by means of the Bloch equations, the temporal progression of longitudinal and transverse magnetization can be assessed. At the steady-state, in the case of flip back deactivation (FB OFF), we have:

$$M_{xy}^{Steady\_State} = M_z^0 \cdot \left(1 - e^{-[TR-(ETL \cdot \Delta TE)]/T_1}\right) \qquad [5]$$

while in the case of flip back activation (FB ON):

$$M_{xy}^{Steady\_State} = M_z^0 \cdot \frac{\left(1 - e^{-[TR-(ETL+1)\cdot \Delta TE)]/T_1}\right)}{\left(1 - e^{-(ETL+1)\cdot \Delta TE/T_2} \cdot -e^{-[TR-(ETL+1)\cdot \Delta TE]/T_1}\right)} \qquad [6]$$

Eq. [6] accounts for the augmented steady-state magnetization due to the addition of the residual transverse magnetization flipped back on z after a time from the initial 90° radiofrequency (RF) pulse equal to [TR-(ETL + 1)]. More details can be found in (33,34). It is worth noticing that the first ETL echoes are considered for image formation, while at the time of the (ETL + 1) echo the driven equilibrium pulse is delivered.

By substituting Eq. (5) or Eq. (6) in Eq. (4) we obtain expressions useful to compare the SNR achievable

with different RARE settings (TR, ETL, FB) given the spin system relaxation times ($T_1$ and $T_2$). This relation cannot be used to predict absolute SNR and detection thresholds until it is based on uncalibrated signal and noise levels. Still, it permits predicting the optimal settings and percent losses for suboptimal parameters. Moreover, it predicts SNR variations due to changes in relaxation times, provided that the other scanner, sequence, and object factors determining the signal and noise levels are unchanged.

In Eq. (4), acquisition parameters BW, $N_{freq}$, $N_{phase}$, $\Delta x$, $\Delta y$, $\Delta z$, and TA were fixed. Importantly, comparisons were performed at equal acquisition time TA, translating faster TR into increased averaging. In this way, the tradeoff between signal loss and increased signal accumulation at different TR and ETL settings was explored. The rationale is in the limits of TA to be set in in vivo studies, which represent the final goal of these imaging methods. Numerical simulations were performed in MatLab (MathWorks, Natick, MA). In a first evaluation, the SNR was mapped vs. TR (range 0.3–6.0 sec) and ETL (1,2,4,8,16,32) with both FB ON and FB OFF at four different combinations of ($T_1$, $T_2$): (5, 2.5 sec), (5, 0.7 sec), (1, 0.2 sec), (0.5, 0.2 sec).

Optimal scan parameters and SNR losses at suboptimal parameters were assessed for each ($T_1$, $T_2$) combination. Furthermore, the dependence of the optimal SNR value on ($T_1$, $T_2$) values was assessed. In a second evaluation, in order to provide a general rule to optimize ETL and TR to yield maximum SNR, optimal parameter maps were developed by varying $T_1$ and $T_2$ in a wider range: $T_1$ (0.3 sec to 4 sec) and $T_2$ (0.05 sec to 1 sec). $\Delta$TE was fixed to 11.6 msec. The aim of the analysis is twofold: 1) to show the improvement in SNR on a specific $^{19}$F reporter by optimizing the acquisition parameters TR, ETL, and FB according to $T_1$, $T_2$; 2) to compare the SNRs on reporters with different magnetic properties ($T_1$, $T_2$).

## Experimental Design

### Scanner Description

The experiments were performed on a BioSpec 70/30 USR (Bruker, Ettlingen, Germany) preclinical MRI scanner. The system has a magnetic field strength of 7T and a 30-cm bore diameter. The scanner is equipped with an actively shielded gradient system with integrated shims set up to second order. The maximum gradient amplitude is 400 mT/m. Studies of $^1$H MRI, $^{19}$F MRI, and $^{19}$F MRS were carried out using a transceiver double-tunable $^1$H/$^{19}$F linear birdcage RF coil having a diameter of 72 mm. All measurements were done at room temperature.

### In Vitro Phantoms and Ex Vivo Brain Preparation

$^{19}$F-MRI acquisitions were carried out on $KPF_6$ in different conditions:

- Water solution phantom. Five test tubes (1 cm diameter, 1 mL) containing water solutions of $KPF_6$ at different concentrations were considered: 0.432 M (saturation), 0.1 M, 0.05 M, 0.01 M, and 0.005 M.
- Agarose phantom. A test tube containing a mixture of agarose and $KPF_6$ with a concentration 0.0142 M was considered.
- Ex vivo brain preparation (36). Guinea pig brain was maintained in vitro by means of an arterial perfusion of a carboxygenated (95% $O_2$, 5% $CO_2$) saline solution (composition: 126 mM NaCl, 3 mM KCl, 1.2 mM $KH_2PO_4$, 1.3 mM $MgSO_4$, 2.4 mM $CaCl_2$, 26 mM $NaHCO_3$, 15 mM glucose, 2.1 mM HEPES, and 3% dextran M.W. 70,000, pH = 7.3, T° 32 C). The $KPF_6$ solution was coperfused along with the complex saline solution for 15 minutes, and thereafter washed out for 2 minutes. At the end, brain was fixed in agar 6% by immersion.

All concentrations are referred to as $KPF_6$, which means a 6-fold concentration of $^{19}$F.

### Scanner Adjustments and Object Settings

Phantoms were placed on a rat bed and inserted in the magnet bore in correspondence with the RF coil center. The usual scanner adjustment on $^1$H spin system was performed working at a frequency of about 300 MHz and included 1) an RF coil tuning and matching procedure, 2) shimming procedure (up to second order), 3) reference pulse gain ($\pi/2$), and 4) receiver gain adjustments. A standard $^1$H imaging protocol was used for assessing the correct positioning of objects in the coil field of view (FOV): gradient-echo FLASH pulse sequence, FOV = $5 \times 5$ cm$^2$, TE = 6 msec, TR = 0.1 sec, slice thickness = 2 mm, matrix = $128 \times 128$, flip angle = 30°, NA = 1, TA = 12 sec.

A further tuning step for $^{19}$F spin systems was carried out. Since $KPF_6$ concentrations in the considered samples did not provide a signal level sufficient for the automatic adjustment of the reference pulse gain, a highly concentrated sample containing 2 mL of pure (ie, 13 M) TFE (2,2,2,trifluoroethanol) was added in the FOV. TFE displayed a single isochrome at −77.3 ppm (282.5704 MHz at 7T), close to the central frequency of the $KPF_6$ spectrum, which in turn displayed two isochromes separated by ~2.5 ppm (ie, 0.706 kHz). Adjustments performed at the TFE frequency were considered valid for scans performed at the $KPF_6$ central frequency. The shimming procedure was not repeated and the receiver gain was set to the maximum available value (203 dB).

Slices for the $^{19}$F MRI acquisition were selected on $T_2$-weighted spin-echo axial $^1$H MR images acquired at 300 MHz with TE = 11.6 msec, FOV = $4.2 \times 4.2$ mm$^2$, matrix = $128 \times 128$ (nominal in-plane resolution 0.0328 mm$^2$), slice thickness = 5 mm, NA = 2, TA = 1 min 20 sec.

## RARE Pulse Sequence: Experimental Assessment and Optimal Parameters for $^{19}$F Compounds

### Image and Data Analysis

To estimate the SNR, images were segmented into object and background by means of Otsu's method (37). Signal was evaluated as the mean of the whole segmented object. Noise was computed as standard

deviation in four regions ($8 \times 8$ pixel, each) at background corners. The SNR was evaluated as mean signal/noise standard deviation.

Fusion of $^{1}H$ and $^{19}F$ MRI for the brain preparation was performed by superimposition (ImageJ, NIH, Bethesda, MD, http://rsbweb.nih.gov/ij/).

### *Linearity*

Linearity vs. $^{19}F$ concentration was evaluated on the water-$KPF_6$ phantoms (concentrations: 0.1 M, 0.05 M, 0.01 M, 0.005 M) with a RARE pulse sequence with the following parameters: FOV = $5 \times 5$ cm$^2$, $\Delta$TE = 4 msec, TR = 2500 msec, ETL = 8, slice thickness = 3 mm, matrix = $32 \times 32$, TA = 1 h 23 min, NA = 500.

### *$^{19}F$ MRS Relaxation Analysis*

$T_1$ and $T_2$ relaxation times of $KPF_6$ systems were measured by means of an MRS total volume approach. $T_1$ relaxation time was estimated using the inversion recovery technique with the following parameters: size of FID 16,384 points, number of scans (NS) = 10, spectral width (SW) = 11.68 ppm/3301Hz, dwell time (DT, sampling time) = 151 $\mu$s, relaxation delay (D1, time before each inversion pulse) = 10 sec, TI (0.1, 0.2, 0.5, 1, 3, 5, 10, 20, 30, 40 sec), pulse length = 130 $\mu$s and 260 $\mu$s, TA = 35 min. $T_2$ relaxation time was estimated using a Carr-Purcell-Meiboom-Gill (CPMG) sequence with the following parameters: size of FID 16,384 points, NS = 8, SW = 11.68 ppm/3301Hz, DT = 151 $\mu$s, D1 = 10 sec, TE = (0.04, 0.16, 0.32, 0.640, 1.28, 2.56, 5.12, 10.24 sec), pulses length = 130 $\mu$s and 260 $\mu$s, TA = 14 min. The relaxation curves were fitted using TOPSPIN (Bruker, Germany).

### *Experimental Validation of the Theoretical Assessments for RARE Parameters Optimization*

For each of the three $KPF_6$ samples (water phantoms, agarose phantom, and ex vivo brain preparation), the theoretical SNR provided by Eq. [7] was mapped vs. TR and ETL with both FB ON and FB OFF, by using the experimentally derived $T_1$ and $T_2$ time constants.

Then, for each sample the maximum SNR was individuated (SNRo) and three combinations of parameters (TR, ETL, and FB) corresponding to three different SNR levels (high-SNR = point above 90% of SNRo; medium-SNR = point between 75% and 90% of SNRo, SNR loss $\approx$20%; low-SNR = point between 50% and 75% of SNRo, SNR loss $\approx$40%) were chosen and adopted in experimental RARE acquisitions.

Experimental RARE acquisitions were performed with the following parameters: BW = 50 kHz, FOV = $4.2 \times 4.2$ cm$^2$, TE = 11.6 msec, number of slices = 1 for water solution and agarose and 8 for ex vivo brain, slice thickness = 2 mm for water solution and 5 mm for agarose and ex vivo brain, data matrix = $32 \times 32$ (nominal resolution $1.313 \times 1.313$ mm$^2$). The acquisition time was 1 hour for water solution phantom and agarose phantom and 2 hour for ex vivo-brain preparation. A zero fill acceleration *k*-space encoding strategy was used, (ZF4, $N_{freq} = 32$, $N_{phase} = 8$, voxel size = 34.45 mm$^3$) for agarose and ex vivo brain preparation. A centric *k*-space encoding order was used. In each condition, the relative variations in experimental SNR were assessed and compared with those theoretically predicted.

### *Optimized RARE Sensitivity Limit*

Once assessed, the optimal RARE parameters for $KPF_6$ in water (TR = 0.7 sec – ETL = 8), the sensitivity limit of the acquisition system was evaluated by progressively reducing the concentration of $KPF_6$ phantoms in water (10 mM, 5 mM, 1 mM, 0.5 mM) and acquiring images using the following parameters: TA = 2 hours, FOV = $4.2 \times 4.2$ cm, matrix $32 \times 32$ slice thickness 5 mm, ZF4 (voxel size 34.45 mm$^3$). The SNR in experimental images was estimated as the ratio between the average intensity in the object ROI and the noise STD in four background ROIs at the image corners ($8 \times 8$ pixels each).

## RESULTS

### *RARE Pulse Sequence: Theoretical Assessment of SNR and Optimal Parameters*

In Fig. 1, changes in the SNR as a function of TR and ETL for the four considered couples of ($T_1$, $T_2$) relaxation times are shown with FB ON (left) and with FB OFF (right).

It can be observed that the lowest SNRs were obtained when $T_1$ and $T_2$ reached the maximum ratio (Fig. 1b, right panel, $T_1 = 5$ sec, $T_2 = 0.7$ sec) and with FB OFF. In this case, the optimal TR was found at 6 sec and the optimal ETL at 32, corresponding to an SNRn = 0.45; ie, with a loss of 55% with respect to the most favorable condition, SNRref.

Values of optimal TR and ETL together with the corresponding SNRn for each of the considered $T_1$, $T_2$ combinations (with FB ON and OFF) are displayed in Table 1.

From the displayed analysis it can be noticed that:

- Flip back pulse activation (FB ON) generally provides an improvement in SNR. The improvement is obviously more evident for long $T_1$ and $T_2$ values, corresponding to a low longitudinal magnetization and to a high residual transverse magnetization in TR.
- Negligible loss is caused by long $T_1$, provided a sufficient ETL is set and FB is activated (FB ON).
- The achievable SNR decreases if $T_1/T_2$ ratio increases.

A general rule to optimize ETL and TR as a function of the $^{19}F$ compound can be derived, by examining the optimal parameter reported in Fig. 2 and Table 2. These were obtained by varying $T_1$ in the range (0.3 sec to 4 sec) and $T_2$ in the range (0.05 sec to 1 sec). In Fig. 2 the optimal parameters (ETL, TR) are displayed for both FB ON and FB OFF conditions.

It can be observed that in case of driven equilibrium pulse (FB ON) the optimal ETLs are lower compared to FB OFF.

As clearly shown in Fig. 2a,c, in both conditions ETL increases with $T_2$. Considering FB OFF, the optimal TR is almost proportional to $T_1$ (Fig. 2d), since it

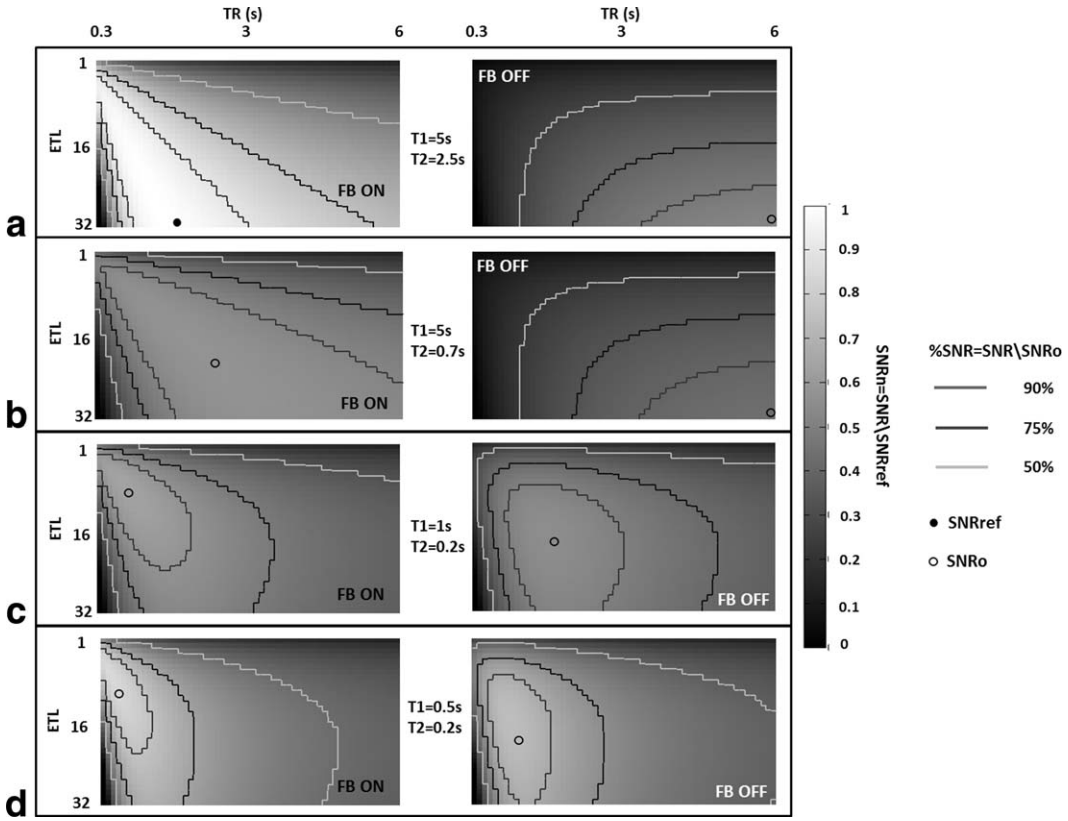


**Figure 1.** SNRn = SNR/SNRref (grayscale) maps in (TR, ETL) parametric space with different ($T_1$, $T_2$) combinations (top to bottom). SNR values computed with Eqs. 8–10 are normalized with respect to the absolute maximum value (SNRref). The reference value SNRref is the maximum obtained SNR, marked by the closed circle in the upper left panel (a) was obtained with TR = 1.6 sec, ETL = 32, and FB ON for the simulated reporter having $T_1 = 5$ sec and $T_2 = 2.5$ sec. FB ON and FB OFF conditions are considered in the left and right columns, respectively. In each panel, %SNRo values compared to the optimal point (open circle, SNRo) are enlightened by the contour maps: 90% (red), 75% (blue), 50% (green). The forbidden zone TR<(ETL+1)*TE is marked in black.

reflects the optimal balance between the signal loss and the increase in the number of averages by shortening the saturation recovery. With FB ON the dependence of the optimal TR vs. $T_1$ is instead not trivial (Fig. 2b), since longitudinal magnetization recovered after $T_2$ decay is accounted for, according to TE and ETL.

In Table 2 the optimal parameters are presented for FB ON and for a series of ($T_1$, $T_2$) values.

### *RARE Pulse Sequence: Experimental Assessment and Optimal Parameters for $^{19}F$ Compounds*

#### *Linearity*

The results shown in Fig. 3 display a high linear correlation ($r > 0.99$) between SNR and $^{19}F$ concentration. Interestingly, a good SNR level (11.00) was obtained with a modest acquisition time even for the lowest concentration, 5 mM. Note that this preliminary evaluation uses a RARE sequence not yet optimized and with a full *k*-space sampling. The lowest concentration explored is one order of magnitude higher than that reached with the optimized sequence (see last paragraph or Results).

#### *$^{19}F$ MRS Relaxation Analysis*

The $KPF_6$ water solution displayed $T_1 = 4.039 \pm 0.037$ sec and $T_2 = 1.061 \pm 0.010$ sec; the mixture of agarose and $KPF_6$ had a $T_1$ of $4.090 \pm 0.238$ sec and a $T_2$ of $0.052 \pm 0.001$ sec; finally, the ex vivo $KPF_6$ preparation had a $T_1$ of $3.519 \pm 0.273$ sec and a $T_2$ of $0.062 \pm 0.004$ sec. $T_1$ changes were not considerable, with a slight increase of 14% in agarose compared to ex vivo brain preparation. Conversely, $T_2$ displayed a remarkable drop in agarose (−95%) and in the brain ex vivo preparation (−94%) compared to the water solution.

#### *Experimental Validation of the Theoretical Assessments for RARE Parameters Optimization*

The results obtained with Eq. [7] by using the estimated relaxation times for the three different

Table 1
Optimal TR-ETL and Corresponding SNRn Provided by the Theoretical Analysis of the RARE Sequence, for Four Different Combinations of $T_1$ and $T_2$

| RELAXATION TIMES | FB ON | | FB OFF | |
|---|---|---|---|---|
| *T1 (s) – T2 (s)* | *TR (s) – ETL* | *SNRn* | *TR (s) – ETL* | *SNRn* |
| 5-2.5 | 1.6–32 | 1 | 6–32 | 0.525 |
| 5-0.7 | 2.4–21 | 0.576 | 6–32 | 0.436 |
| 1-0.2 | 0.8–9 | 0.639 | 1.7–18 | 0.554 |
| 0.5-0.2 | 0.5–9 | 0.849 | 1–17 | 0.742 |

Table 2
Optimal Parameters (ETL,TR) for Different $T_1$-$T_2$ Combinations With FB ON

| | T2 (s) | | | | |
|---|---|---|---|---|---|
| T1 (s) | 0.2 | 0.4 | 0.6 | 0.8 | 1 |
| 0.2 | ETL = 8<br>TR = 0.3 | n.a. | n.a. | n.a. | n.a. |
| 1.2 | ETL = 8<br>TR = 0.8 | ETL = 12<br>TR = 0.8 | ETL = 17<br>TR = 0.8 | ETL = 19<br>TR = 0.8 | ETL = 21<br>TR = 0.8 |
| 2.1 | ETL = 8<br>TR = 1.2 | ETL = 13<br>TR = 1.2 | ETL = 18<br>TR = 1.2 | ETL = 20<br>TR = 1.2 | ETL = 23<br>TR = 1.2 |
| 3.1 | ETL = 8<br>TR = 1.7 | ETL = 13<br>TR = 1.6 | ETL = 17<br>TR = 1.6 | ETL = 23<br>TR = 1.6 | ETL = 26<br>TR = 1.6 |
| 4 | ETL = 9<br>TR = 2.3 | ETL = 14<br>TR = 2 | ETL = 17<br>TR = 2 | ETL = 23<br>TR = 2 | ETL = 26<br>TR = 2 |

environments and with FB ON are shown in Fig. 4, left panels. Inside each panel, displayed SNR values were normalized by the specific panel maximum value (SNRo, open circles), since no comparison among the different preparations was scheduled, due to different concentrations and volumes.

The parameters corresponding to high-SNR (H, close to optimum), medium-SNR (M, SNR loss ≈20%), and low-SNR (L, SNR loss ≈40%) conditions are reported in Table 3. Parameters were chosen in order to provide a simulated SNR value in the H, M, L range, respectively, at values compatible with settings allowed by the scanner in experimental acquisition.

Experimental images of fluorinated water solution phantom, mixture of agarose and $KPF_6$ and guinea pig brain preparation corresponding to the high-SNR parameters are shown in the right panels of Fig. 4. The image of the perfused brain is also shown in Fig. 5, superimposed to the $^1$H-MR anatomical image.

In Table 4, the theoretical %SNRo (Sim, normalized by the theoretical optimum) and the experimental SNR (Exp, values estimated from images) are

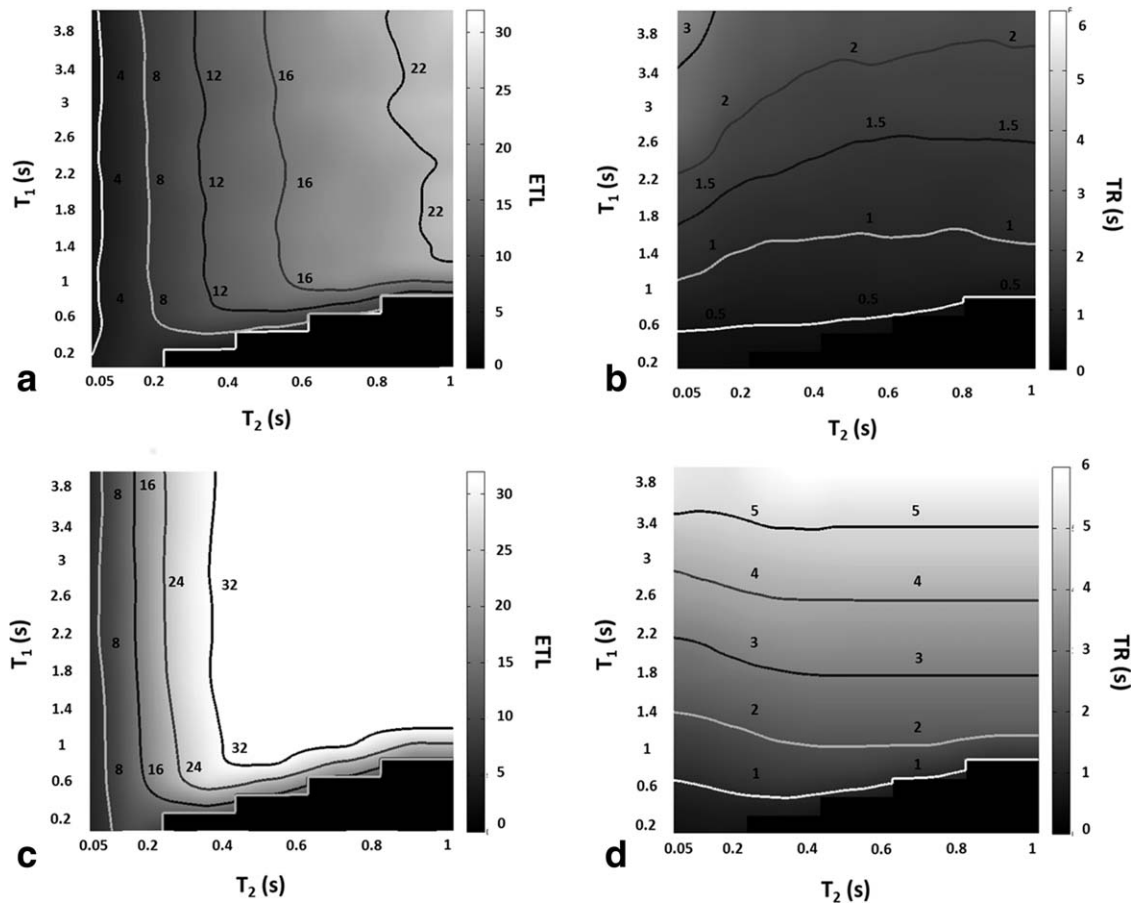


**Figure 2.** Optimal parameters maps (ETL and TR) are shown in parametric space for different $T_1$ and $T_2$. RARE sequence optimization with FB ON (**a**,**b**) and FB OFF (**c**,**d**) is displayed. A wide range of relaxation times $T_1$ (0.2–4 s) and $T_2$ (0.05–1 s) was considered. A ΔTE of 11.6 msec was chosen.

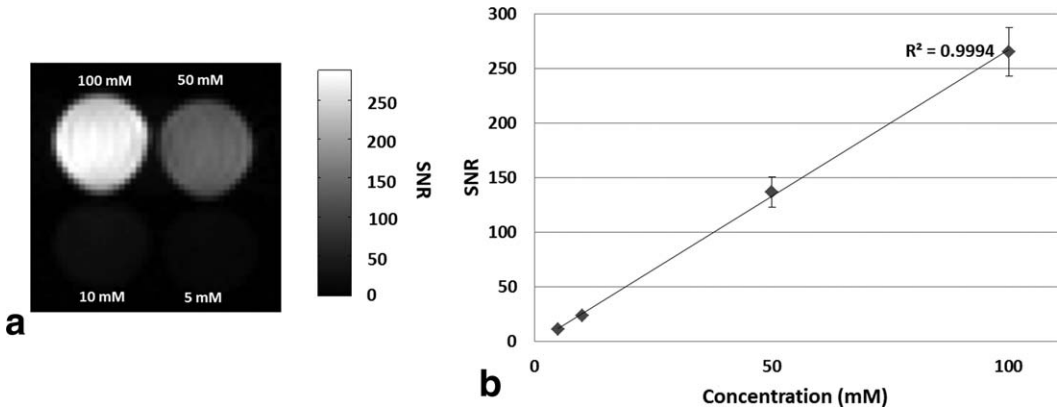


**Figure 3.** $^{19}$F MRI of $KPF_6$ water solution phantoms at different concentrations (a) and linearity assessment of RF volume coil (b). SNR vs. molar concentration is reported. The SNR of the experimental points in panel (b) is referred to the corresponding image in panel (a). SNR map is shown (a). For SNR estimation ROIs were manually selected on phantoms at different concentrations and the standard deviation of the background was considered as noise.

represented for the high-SNR, medium-SNR, and low-SNR condition, together with the %SNR loss compared to the relevant high-SNR condition. A good accordance of real SNR losses due to nonoptimal scan parameterization compared to those theoretically predicted is displayed (Model error column): the prediction of SNR in real acquisition according to the simulation model was made considering a loss proportional to the theoretical one; the error was obtained by subtracting the experimental value from the predicted one and was finally normalized by the respective high experimental SNR value.

*Optimized RARE Sensitivity Limit*

The detection limit for the optimal RARE setting was reached in a water solution on $KPF_6$ with a concentration 0.5 mM, corresponding to $6.22 \times 10^{16}$ fluorine atoms per voxel and to a SNR of $3.42 \pm 0.77$.

## DISCUSSION

$^{19}$F MRI is a millimolar concentration technique (8,9). $^{19}$F MRS can reduce this threshold to micromolar concentration (38) but does not permit spatial localization of $^{19}$F compounds. Increasing the sensitivity of $^{19}$F MR methods is therefore a major goal for molecular imaging applications. In this work a procedure for optimizing the SNR on $^{19}$F-MR RARE images was addressed, with consideration of the limited acquisition times needed for in vivo preclinical experiments, and the high differences in relaxation times depending on the molecular reporter and its biological

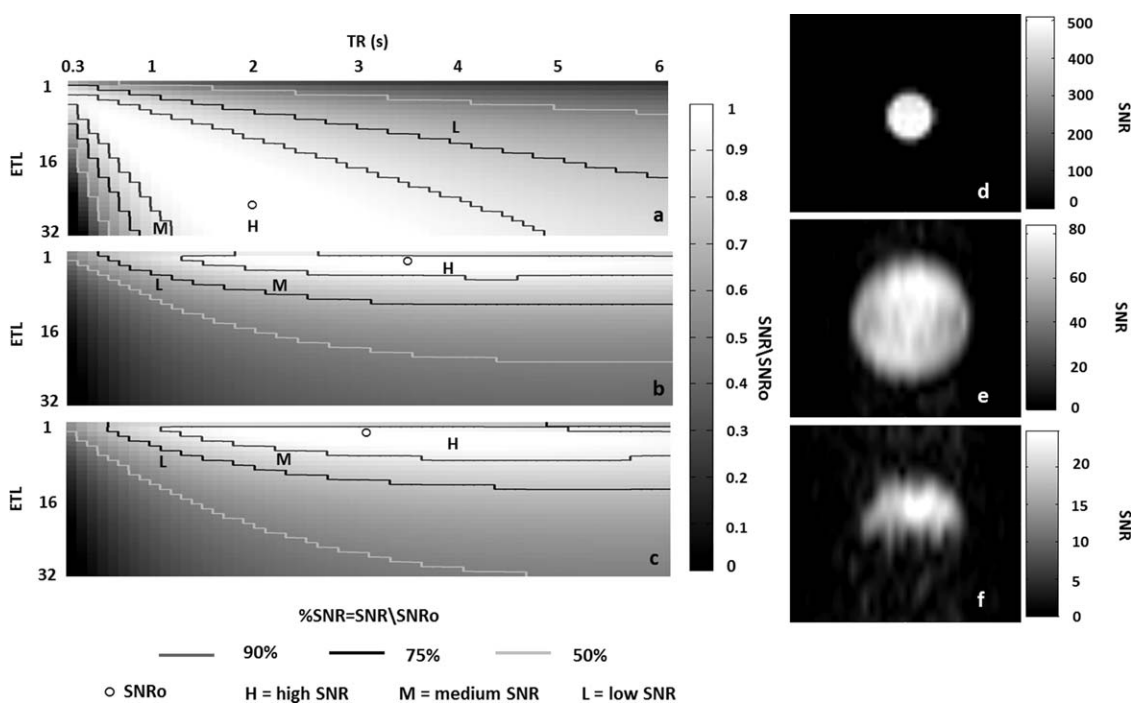


**Figure 4.** Left panels: SNR maps in (TR, ETL) parametric space generated by using the experimental values of $T_1$ and $T_2$: (a) $KPF_6$ in water solution (432 mM), (b) $KPF_6$ in agarose, (c) $KPF_6$ perfused in guinea pig brain. Right panels: corresponding $^{19}$F MR images experimentally obtained with high-SNR parameters.


**Figure 5.** $^{1}H$ MRI of ex vivo guinea pig brain at high resolution (**a**). $^{19}F$ MRI acquired during the same session at lower resolution (**b**). Superimposition of anatomical reference and $KPF_6$ distribution (**c**).

Table 3
Parameters Used for Experimental $^{19}F$ MR Images

| PHANTOMS ($KPF_6$) | Parameters: TR/ETL | | |
|---|---|---|---|
| | *SNR-High* | *SNR-Medium* | *SNR-Low* |
| Water | 1.75 s / 32 | 0.8 s / 32 | 4 s / 8 |
| Agar | 3.75 s / 4 | 2.25 s /8 | 1 s / 8 |
| Brain | 3.75 s / 4 | 2.25 s /8 | 1 s / 8 |

environment. Starting from a theoretical assessment, the proposed method derives an empirical relationship describing the dependence of the relative SNR on sequence parameters and compound magnetic properties. This relationship allows predicting optimal settings for specific compounds. Parameters mapped for optimization are those primarily adjusted in RARE: TR, ETL, and the use or not of driven equilibrium pulses. Optimization maps are provided for chosen fixed TE and for the other machine-dependent parameters imposed by our setting; nonetheless, the proposed method can be easily implemented for different scanners.

The experimental analysis of $KPF_6$ in the considered preparations (water, agarose, and guinea pig brain) confirmed the long $T_1$ decay times of low molecular weight compounds (19,20). Further analysis of $T_2$ relaxation time confirmed the dramatic changes moving from pure water solutions to macromolecular in vitro environments (in our case agarose) and biological tissue (fixed brain), thus displaying the necessity of specific setting adaptations.

The proposed simulation of RARE sequence according to $T_1$ and $T_2$ was able to: 1) provide SNR maximization rules, and 2) give reliable forecasts of SNR improvements compared to nonoptimal parameter settings, which were validated in the experimental acquisitions.

The method can be easily generalized by constructing optimization maps specific to a given marker (characterized by $T_1$ and $T_2$) and to other machine-dependent settings such as BW and TE (18), gradient delays, and timing of RF pulses. The use of the minimum echo time achievable is necessary to increase the SNR. Interestingly, the maps considered in this work show that a proper setting of RARE parameters permits an SNR gain up to 30%.

Moreover, a comparison of simulated SNR maps for different $T_1$ and $T_2$ allows us to predict the performance of different reporters or of a given reporter in different environments, thus providing a valuable framework in designing new molecules as to their magnetic properties and their response to background.

However, at the current stage, several limitations of the work should be noted. First, our experiments did not permit validating absolute SNR comparison in different conditions, since the considered preparations differed by concentration and concentration distribution of the $^{19}F$ reporter, not permitting quantitative comparisons. Further work with different reporters and different preparations is therefore needed.

Second, the extension to clinical applications is currently restricted by many factors: 1) the long scanning time may be an issue, 2) the use of long echo trains increases dramatically the RF power deposition, and consequently the specific absorption rate (SAR). Possibly, a method extension to low refocusing flip angles can reduce SAR with limited SNR loss (39,40). A further limitation of the present work is the use of a fluorinated marker not suited to in vivo studies and in this sense the results must be considered as preliminary. Nonetheless, the applied theoretical model appears to be of large generality and applicability, since it is based on Bloch equations, simple considerations over $T_1/T_2$ relaxations times, and basic features of RARE sequences.

Finally, the method adopted to assess $T_1$, $T_2$ relaxation times can be used even for in vivo studies considering the limited acquisition time (less than 1 hour, for both $T_1$ and $T_2$ estimation), provided that the whole volume is addressed and the fluorinated marker has achieved a large concentration in target

Table 4
Comparison of Simulated and Real SNR Drops When Deviating From Optimal Settings (High-SNR)

| PHANTOMS ($KPF_6$) | High – SNR | | Medium – SNR | | | | | Low – SNR | | | | |
|---|---|---|---|---|---|---|---|---|---|---|---|---|
| | | | *Sim* | | *Exp* | | *Model* | *Sim* | | *Exp* | | *Model* |
| | *Sim %SNRo* | *Exp SNR* | *%SNRo* | *SNR loss* | *SNR* | *SNR loss* | *Error* | *%SNRo* | *SNR loss* | *SNR* | *SNR loss* | *Error* |
| Water | 97 | 434 | 77 | −20.6% | 356 | −18.0% | **−2.6%** | 59 | −39.2% | 302 | −30.4% | **−8.8%** |
| Agar | 97 | 57.86 | 75 | −22.7% | 47.12 | −18.6% | **−4.1%** | 56 | −42.3% | 37.35 | −35.4% | **−6.8%** |
| Brain | 98 | 12.02 | 82 | −16.3% | 9.70 | −19.3% | **3.0%** | 62 | −36.7% | 7.35 | −38.9% | **2.1%** |

Water (solution), agar (solution), brain (ex vivo) refer to the three experimented preparations with $KPF_6$; see text.
igh-SNR = condition closest to optimum; medium-SNR = suboptimal condition chosen with a loss ≈ 20%; low-SNR = suboptimal condition with a loss ≈ 40%, Sim = theoretical %SNRo normalized to the specific optimal point, Exp = SNR in experiments (adimensional units). SNR loss = % decrease in SNR compared to high-SNR condition, computed and measured in Sim and Exp, respectively. Model error = % forecast error in the Exp SNR loss compared to Sim SNR loss.

regions, where these parameters can be considered homogeneous. Conversely, the proposed methodology is likely to provide poor results in the presence of diffused distributions of the fluorinated marker into different tissues largely affecting $T_1$ and $T_2$ values; nonetheless, this is not a condition commonly aimed at in molecular imaging, where targeting of specific structures is most often the main goal.

In conclusion, the use of fluorinated molecular reporters in MRI, although a promising technique, demands acquisition strategies properly adapted for different reporters and environments. Fast spin echo sequences permits dealing with a broad range of relaxation times, provided that a proper tuning of their parameters is performed. Relationships empirically drawn from simulations are proposed as a simple tool for a proper tuning of the RARE sequence, to be inserted into an acquisition protocol reliable and target-specific.

A further value of the proposed approach is foreseen in the construction of new fluorinated reporters, which is not only subject to biomolecular considerations (transport, selectivity to target, toxicity, etc.), but is also highly conditioned by relaxation times.

## REFERENCES


1. Sosnovik DE, Weissleder R. Emerging concepts in molecular MRI. Curr Opin Biotechnol 2007;18:4–10.
2. Hoehn M, Himmelreich U, Kruttwig K, Wiedermann D. Molecular and cellular MR imaging: potentials and challenges for neurological applications. J Magn Reson Imaging 2008;27:941–954.
3. Bonnet CS, Toth E. Smart MR imaging agents relevant to potential neurologic applications. AJNR Am J Neuroradiol 2010;31: 401–409.
4. Himmelreich U, Dresselaers T. Cell labeling and tracking for experimental models using magnetic resonance imaging. Methods 2009;48:112–124.
5. Srinivas M, Heerschap A, Ahrens ET, Figdor CG, de Vries IJ. 19F MRI for quantitative in vivo cell tracking. Trends Biotechnol 2010;28:363–370.
6. Chen J, Lanza GM, Wickline SA. Quantitative magnetic resonance fluorine imaging: today and tomorrow. Wiley Interdiscip Rev Nanomed Nanobiotechnol 2010;2:431–440.
7. Janjic JM, Ahrens ET. Fluorine-containing nanoemulsions for MRI cell tracking. Wiley Interdiscip Rev Nanomed Nanobiotechnol 2009;1:492–501.
8. Ruiz-Cabello J, Barnett BP, Bottomley PA, Bulte JW. Fluorine (19F) MRS and MRI in biomedicine. NMR Biomed 2011;24:114–129.
9. Srinivas M, Boehm-Sturm P, Figdor CG, de Vries IJ, Hoehn M. Labeling cells for in vivo tracking using (19)F MRI. Biomaterials 2012;33:8830–8840.
10. Ahrens ET, Flores R, Xu H, Morel PA. In vivo imaging platform for tracking immunotherapeutic cells. Nat Biotechnol 2005;23:983–987.
11. Higuchi M, Iwata N, Matsuba Y, Sato K, Sasamoto K, Saido TC. 19F and 1H MRI detection of amyloid beta plaques in vivo. Nat Neurosci 2005;8:527–533.
12. Flogel U, Ding Z, Hardung H, et al. In vivo monitoring of inflammation after cardiac and cerebral ischemia by fluorine magnetic resonance imaging. Circulation 2008;118:140–148.
13. Ruiz-Cabello J, Walczak P, Kedziorek DA, et al. In vivo "hot spot" MR imaging of neural stem cells using fluorinated nanoparticles. Magn Reson Med 2008;60:1506–1511.
14. Ebner B, Behm P, Jacoby C, et al. Early assessment of pulmonary inflammation by 19F MRI in vivo. Circ Cardiovasc Imaging 2010;3:202–210.
15. Boehm-Sturm P, Mengler L, Wecker S, Hoehn M, Kallur T. In vivo tracking of human neural stem cells with 19F magnetic resonance imaging. PLoS One 2011;6:e29040.
16. Nelson TR, Newman FD, Schiffer LM, Reith JD, Cameron SL. Fluorine nuclear magnetic resonance: calibration and system optimization. Magn Reson Imaging 1985;3:267–273.
17. Gong BZ, Gill M, Washburn DB, Davenport WC, Adams D, Kwock L. Parameter optimization and calibration of 19F magnetic resonance imaging at 1.5 Tesla. Magn Reson Imaging 1991;9: 101–106.
18. Chalmers KH, Kenwright AM, Parker D, Blamire AM. 19F-lanthanide complexes with increased sensitivity for 19F-MRI: optimization of the MR acquisition. Magn Reson Med 2011;66:931–936.
19. Mizukami S, Takikawa R, Sugihara F, et al. Paramagnetic relaxation-based 19f MRI probe to detect protease activity. J Am Chem Soc 2008;130:794–795.
20. Sotak CH, Hees PS, Huang HN, Hung MH, Krespan CG, Raynolds S. A new perfluorocarbon for use in fluorine-19 magnetic resonance imaging and spectroscopy. Magn Reson Med 1993;29:188–195.
21. Nitz WR. Fast and ultrafast non-echo-planar MR imaging techniques. Eur Radiol 2002;12:2866–2882.
22. Hennig J. K-space sampling strategies. Eur Radiol 1999;9:1020–1031.
23. Srinivas M, Morel PA, Ernst LA, Laidlaw DH, Ahrens ET. Fluorine-19 MRI for visualization and quantification of cell migration in a diabetes model. Magn Reson Med 2007;58:725–734.
24. Bornert P, Norris DG, Koch H, Dreher W, Reichelt H, Leibfritz D. Fast perfluorocarbon imaging using 19F U-FLARE. Magn Reson Med 1993;29:226–234.
25. Jager LJ, Noth U, Haase A, Lutz J. Half-life of perfluorooctylbromide in inner organs determined by fast 19F-NMR imaging. Adv Exp Med Biol 1994;361:129–134.
26. Noth U, Jager LJ, Lutz J, Haase A. Fast 19F-NMR imaging in vivo using FLASH-MRI. Magn Reson Imaging 1994;12:149–153.
27. Noth U, Morrissey SP, Deichmann R, et al. In vivo measurement of partial oxygen pressure in large vessels and in the reticuloendothelial system using fast 19F-MRI. Magn Reson Med 1995;34: 738–745.
28. Dardzinski BJ, Sotak CH. Rapid tissue oxygen tension mapping using 19F inversion-recovery echo-planar imaging of perfluoro-15-crown-5-ether. Magn Reson Med 1994;32:88–97.
29. Lee H, Price RR, Holburn GE, Partain CL, Adams MD, Cacheris WP. In vivo fluorine-19 MR imaging: relaxation enhancement with Gd-DTPA. J Magn Reson Imaging 1994;4:609–613.
30. Giraudeau C, Flament J, Marty B, et al. A new paradigm for high-sensitivity 19F magnetic resonance imaging of perfluorooctylbromide. Magn Reson Med 2010;63:1119–1124.
31. Schmid F, Höltke C, Parker D, Faber C. Boosting 19F MRI-SNR efficient detection of paramagnetic contrast agents using ultrafast sequences. Magn Reson Med 2012;69:1056–1062.
32. Hennig J, Nauerth A, Friedburg H. RARE imaging: a fast imaging method for clinical MR. Magn Reson Med 1986;3:823–833.
33. van Uijen CM, den Boef JH. Driven-equilibrium radiofrequency pulses in NMR imaging. Magn Reson Med 1984;1:502–507.
34. Busse RF, Riederer SJ, Fletcher JG, Bharucha AE, Brandt KR. Interactive fast spin-echo imaging. Magn Reson Med 2000;44: 339–348.
35. McRobbie DW, Moore EA, Graves MJ, Prince MA. MRI from picture to proton. Cambridge, UK: Cambridge University Press; 2006.
36. de Curtis M, Biella G, Buccellati C, Folco G. Simultaneous investigation of the neuronal and vascular compartments in the guinea pig brain isolated in vitro. Brain Res Brain Res Protoc 1998;3: 221–228.
37. Otsu N. A threshold selection method from gray-level histograms. IEEE Trans Sys Man Cybernet 1979;9:62–66.
38. Reid DG, Murphy PS. Fluorine magnetic resonance in vivo: a powerful tool in the study of drug distribution and metabolism. Drug Discov Today 2008;13:473–480.
39. Hennig J. Multiecho imaging sequences with low refocusing flip angles. J Magn Reson 1988;78:397–407.
40. Alsop DC. The sensitivity of low flip angle RARE imaging. Magn Reson Med 1997;37:176–184.